Title

Type I Interferon Regulates a Coordinated Gene Network to Enhance Cytotoxic T Cell–Mediated Tumor Killing

Journal

Cancer Discovery, 10(3)

ISSN

2159-8274

Authors

Fan, Jun-Bao
Miyauchi, Sayuri
Xu, Hui-Zhong
et al.

Publication Date

2020-03-01

DOI

10.1158/2159-8290.cd-19-0608

Peer reviewed

Published OnlineFirst January 23, 2020; DOI: 10.1158/2159-8290.CD-19-0608

RESEARCH BRIEF

Type I Interferon Regulates a Coordinated Gene Network to Enhance Cytotoxic T Cell–Mediated Tumor Killing

Jun-Bao Fan[1], Sayuri Miyauchi[1], Hui-Zhong Xu[2], Dan Liu[1], Leo J.Y. Kim[3,4], Christoph Burkart[1], Hua Cheng[1], Kei-ichiro Arimoto[1], Ming Yan[1], Yu Zhou[5], Balázs Győrffy[6,7,8], Klaus-Peter Knobeloch[9], Jeremy N. Rich[3], Hu Cang[2], Xiang-Dong Fu[10], and Dong-Er Zhang[1,11]

ABSTRACT

Type I interferons (IFN), which activate many IFN-stimulated genes (ISG), are known to regulate tumorigenesis. However, little is known regarding how various ISGs coordinate with one another in developing antitumor effects. Here, we report that the ISG *UBA7* is a tumor suppressor in breast cancer. *UBA7* encodes an enzyme that catalyzes the covalent conjugation of the ubiquitin-like protein product of another ISG (*ISG15*) to cellular proteins in a process known as "ISGylation." ISGylation of other ISGs, including STAT1 and STAT2, synergistically facilitates production of chemokine-receptor ligands to attract cytotoxic T cells. These gene-activation events are further linked to clustering and nuclear relocalization of STAT1/2 within IFN-induced promyelocytic leukemia (PML) bodies. Importantly, this coordinated ISG–ISGylation network plays a central role in suppressing murine breast cancer growth and metastasis, which parallels improved survival in patients with breast cancer. These findings reveal a cooperative IFN-inducible gene network in orchestrating a tumor-suppressive microenvironment.

SIGNIFICANCE: We report a highly cooperative ISG network, in which UBA7-mediated ISGylation facilitates clustering of transcription factors and activates an antitumor gene-expression program. These findings provide mechanistic insights into immune evasion in breast cancer associated with *UBA7* loss, emphasizing the importance of a functional ISG–ISGylation network in tumor suppression.

[1]Moores UCSD Cancer Center, University of California, San Diego, La Jolla, California. [2]The Salk Institute for Biological Sciences, La Jolla, California. [3]Division of Regenerative Medicine, Department of Medicine, University of California, San Diego, La Jolla, California. [4]Medical Scientist Training Program, School of Medicine, Case Western Reserve University, Cleveland, Ohio. [5]State Key Laboratory of Virology, College of Life Science, Wuhan University, Wuhan, Hubei, China. [6]Department of Bioinformatics, Semmelweis University, Budapest, Hungary. [7]2nd Department of Pediatrics, Semmelweis University, Budapest, Hungary. [8]TTK Lendület Cancer Biomarker Research Group, Budapest, Hungary. [9]Institute of Neuropathology, University of Freiburg, Freiburg, Germany. [10]Department of Cellular and Molecular Medicine, Institute of Genomic Medicine, University of California, San Diego, La Jolla, California. [11]Department of Pathology and Division of Biological Sciences, University of California, San Diego, La Jolla, California.

Note: Supplementary data for this article are available at Cancer Discovery Online (http://cancerdiscovery.aacrjournals.org/).

Current address for H.-Z. Xu: Institute for Advanced Study and School of Physical Science and Technology, Soochow University, Suzhou, Jiangsu, China.

Corresponding Authors: Dong-Er Zhang, Moores UCSD Cancer Center, University of California, San Diego, 3855 Health Sciences Drive, #0815, La Jolla, CA 92093. Phone: 858-822-5372; Fax: 858-822-5433; E-mail: d7zhang@ucsd.edu; and Jun-Bao Fan, Phone: 858-822-5327; E-mail: jbfan@ucsd.edu

Cancer Discov 2020;10:382–93

doi: 10.1158/2159-8290.CD-19-0608

Published OnlineFirst January 23, 2020; DOI: 10.1158/2159-8290.CD-19-0608

INTRODUCTION

The cellular and noncellular components of the tumoral niche create a specific tumor microenvironment (TME), where cells continuously sense danger and damage signaling by extracellular and intracellular pattern recognition receptors (PRR) to balance the acts of the host immune system (1). One key event is the production of type I interferons (IFN) in response to the activation of specific PRRs, such as cyclic GMP–AMP synthase, which plays a central role in regulating TME (2). IFNs activate the JAK–STAT pathway, resulting in the induction of hundreds of IFN-stimulated genes (ISG; ref. 3), many of which remain uncharacterized (4). In general, it is thought that each of these ISGs may activate a pathway, and multiple activated pathways collectively contribute to the overall antitumor effect. However, little is known regarding which ISGs are key drivers to the development of the antitumor effect and how these ISGs might coordinate with one another.

Type I IFNs have been well established to orchestrate both innate and adaptive immune response in cancer (2, 5, 6). This is accomplished by mobilizing diverse cell types in the host immune system, including natural killer cells, dendritic cells, tumor-associated macrophages (TAM), B cells, and T cells (5–7). A critical step in gaining antitumor immunity is to increase the traffic of activated effector T cells, such as cytotoxic $CD8^+$ T cells, to infiltrate into the tumor bed to recognize and kill target cancer cells (2, 7). While playing a central role in regulating T-cell priming and homing in the TME (2), excessive IFN signaling is also known to modulate the TME to disable the antitumor function of effector T cells (8). These complex biological responses likely result from pleiotropic actions of ISGs and various feedback control mechanisms, which appear to be highly dependent on specific tumor contexts (4, 9). Therefore, an important goal in enhancing antitumor immune response is to identify key ISG-mediated pathways that favor the development of an antitumor microenvironment, while minimizing the impact of those with adverse effects.

One such ISG, *UBA7*, encodes an ubiquitin-like modifier-activating enzyme (UBA7, also known as UBE1L) that catalyzes the covalent conjugation of the ubiquitin-like protein product of another ISG (*ISG15*) to additional ISGs as well as other cellular proteins in a process termed "protein ISGylation" (10). ISG15 is conjugated to a host of proteins in response to propagate the effects of IFN stimulation and is known to play a role in antiviral immunity, but the cellular consequence of UBA7-dependent ISGylation in the setting of cancer cells is not completely understood. Here, we uncover a regulatory network in which multiple UBA7-targeted ISGs act in a concerted fashion to activate key chemokines and attract cytotoxic T cells to the tumor bed. These findings reveal a synergistic ISG-mediated cellular program to achieve effective antitumor response in the host.

RESULTS

Evidence for the ISGylation-Activating Enzyme UBA7 as a Tumor Suppressor

Type I IFNs have been well established to have immune-stimulatory functions against malignancies, including breast cancer. To identify ISGs that contribute to IFN's effect in preventing breast cancer progression, we examined the prognostic value of 81 individual ISGs showing correlated expression with *ISG15* and another ISG, *MX1*, because both of them are highly induced by IFN (Supplementary Fig. S1A and S1B). We found that the expression of a subset of ISGs was significantly correlated with favorable relapse-free survival (RFS; Supplementary Fig. S1B; Supplementary Table S1). Interestingly, one of the top ISGs positively correlated with patient survival is *UBA7* (Fig. 1A; Supplementary Fig. S1B). This is in contrast to the lack of positive prognostic value for *MX1* (Supplementary Table S1), supporting the idea that not all ISGs positively contribute to antitumor immunity. Interestingly, *ISG15*, encoding the ubiquitin-like donor for UBA7-mediated ISGylation, was also known to be highly elevated in breast cancer (11). Unlike *UBA7*, however, the induction of *ISG15* was negatively correlated with patient survival (Supplementary Table S1). This likely reflects the multifaceted function of ISG15, as free ISG15 is also responsible for attenuating IFN signaling by stabilizing the deISGylation protease USP18 (12). Importantly, the expression of *UBA7* was associated with favorable RFS in triple-negative breast cancer (Fig. 1B). The association of *UBA7* expression with patient survival was also validated in The Cancer Genome Atlas (TCGA) dataset of patients with breast cancer (Supplementary Fig. S1C). Collectively, these results strongly suggest that *UBA7* may function as a critical tumor-suppressive ISG in breast cancer.

We next modeled the tumor-suppressive function of UBA7 in mice to establish its functional relevance. Previous studies have demonstrated that enhanced IFN signaling significantly changes the TME by increasing T-lymphocyte infiltration, thereby causing significant shrinkage of tumors in the mouse mammary tumor virus (MMTV)–polyomavirus middle tumor antigen (PyVmT) breast cancer model (13, 14). We therefore utilized this well-established mouse model to study the function of UBA7 in breast cancer. In line with a published RNA-sequencing (RNA-seq) dataset (15), we detected increased expression of both *Uba7* and *Isg15* in tumors compared with matched controls at week 10 (Fig. 1C), indicating augmented IFN signaling during tumor progression. Knockout (KO) of *Uba7* in mice did not appear to affect normal mammary development (Supplementary Fig. S2). Although both wild-type (WT) and *Uba7*-deleted (KO) MMTV–*PyVmT* mice developed palpable tumors around week 8, we found that tumors grew faster in KO mice compared with WT mice from week 9 to the endpoint when the mice were euthanized, as indicated by the number of mice that developed tumors more than 0.5 cm (Fig. 1D and E). At week 10, for instance, 90% of KO mice developed large tumors more than 0.5 cm compared with 40% of WT mice (Fig. 1E), and the average volume of the largest tumors in KO mice was approximately 380 mm^3 compared with approximately 100 mm^3 in WT mice (Fig. 1F). Given that UBA7 is the activating enzyme for protein ISGylation, we detected both free ISG15 and ISG15-conjugated proteins in tumor lysates from WT mice at this stage, indicative of active protein ISGylation, whereas only free ISG15 was detected in tumor lysates from KO mice (Fig. 1G). This agrees with the idea that UBA7 is a major activating enzyme responsible for tumor-induced protein ISGylation. We also monitored total tumor burden on these animals by quantifying total tumor weight normalized to body weight at the endpoint and found that KO mice had

Published OnlineFirst January 23, 2020; DOI: 10.1158/2159-8290.CD-19-0608

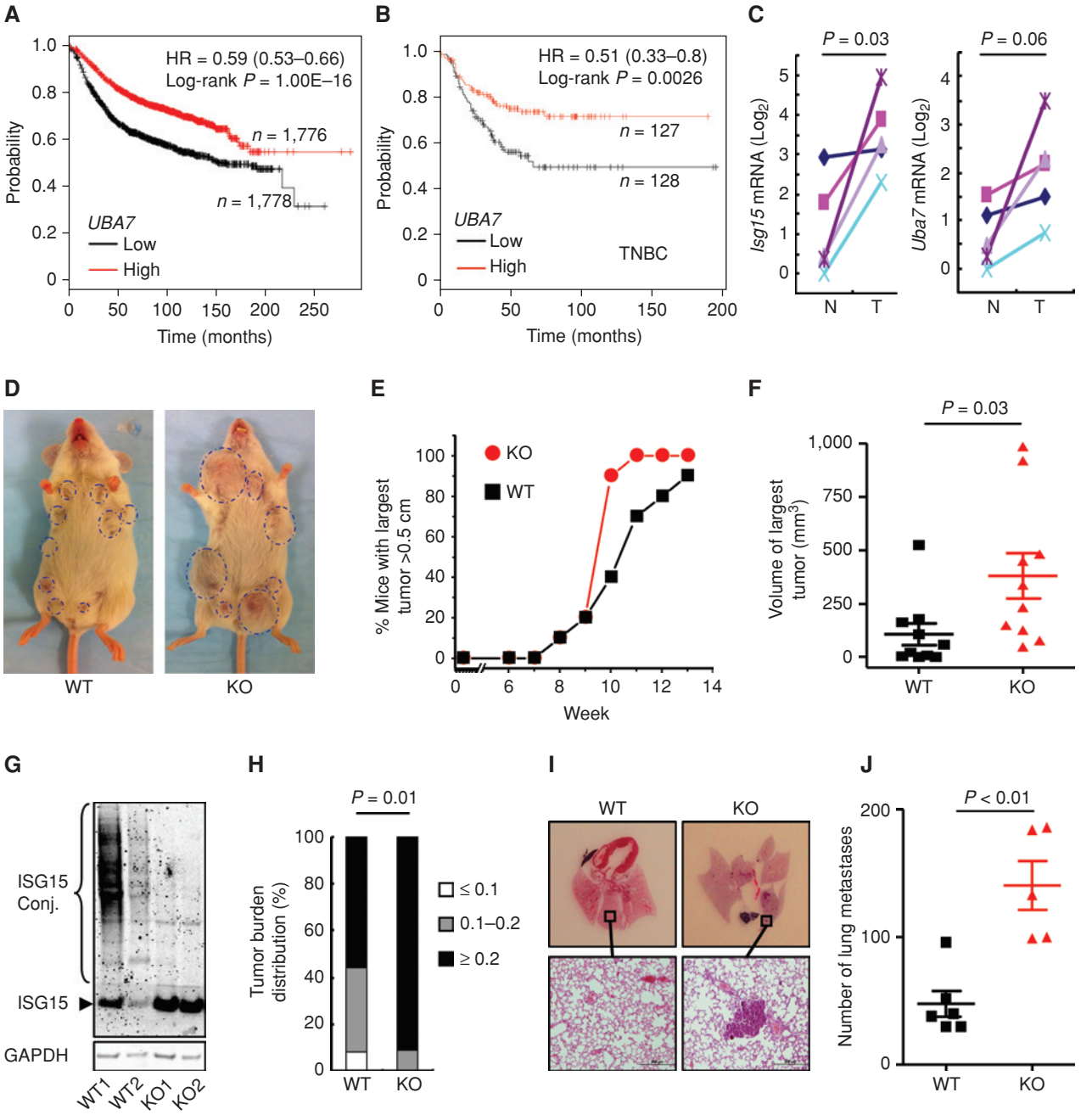

Figure 1. Evidence for the ISGylation-activating enzyme UBA7 as a tumor suppressor. **A,** Kaplan–Meier curves showing the correlation between RFS and *UBA7* expression in breast cancer (Affymetrix ID 203281_at *UBA7*). **B,** Kaplan–Meier curves showing the correlation between RFS and *UBA7* expression in triple-negative breast cancer (TNBC; Affymetrix ID 203281_at *UBA7*). **C,** Expression of *Isg15* and *Uba7* in tumors (T) compared with their adjacent normal (N) tissues from PyVmT/WT mice at 10 weeks of age ($n = 5$). *P*, paired *t* test. **D,** Representative photograph of PyVmT/WT and PyVmT/*Uba7* KO mice at 10 weeks of age. **E,** Percentage of mice with largest tumor diameter above 0.5 cm ($n = 10$/group). **F,** Tumor volume of largest tumors in PyVmT/WT and PyVmT/*Uba7* KO mice at 10 weeks of age ($n = 10$/group). *P*, Student *t* test. **G,** Representative level of ISG15 and protein ISGylation in tumor tissue from PyVmT/WT and PyVmT/*Uba7* KO mice. **H,** Tumor burden (total tumor weight/body weight) distribution of PyVmT/WT ($n = 25$) and PyVmT/*Uba7* KO ($n = 23$) mice at the endpoint. *P*, Fisher exact test. **I** and **J,** Number of spontaneous lung metastasis in PyVmT/WT and PyVmT/*Uba7* KO mice. Serial lung sections were stained with hematoxylin and eosin ($n = 5$–6). *P*, Student *t* test. Scale bars, 500 μm.

more relatively large tumors (those with tumor burden more than 0.2) than WT mice (Fig. 1H). In addition, KO mice also showed increased incidence of lung metastasis (Fig. 1I and J). Collectively, our data on *Uba7* KO mice revealed a tumor-suppressive function of protein ISGylation. To further support this finding, we examined USP18$^{C61A/C61A}$ knock-in (KI) mice in which ISGylation was increased by inactivating the deconjugating enzyme USP18 (16) and found similar suppression to breast tumor growth (Supplementary Fig. S3A–S3C). Together, these results demonstrated that protein ISGylation

Published OnlineFirst January 23, 2020; DOI: 10.1158/2159-8290.CD-19-0608

was tumor-suppressive in the MMTV–PyVmT breast cancer model, which supports the role of *UBA7* as a critical tumor-suppressive ISG in human breast cancer.

Protein ISGylation Stimulates Intratumoral Infiltration of T Lymphocytes

To understand how protein ISGylation suppressed tumor growth, we analyzed genes that were coexpressed with *UBA7* from the TCGA breast cancer dataset. Excluding the expected association of classic ISGs, we found that >600 human genes showed coexpression with *UBA7* (Supplementary Fig. S4A, $R \geq 0.30$). Ingenuity pathway analysis revealed that the top five canonical pathways are all related to T cells (Supplementary Fig. S4B). Interestingly, the chemokine signaling pathway is also revealed by the analysis, and CXCR3, which is mostly expressed on activated T lymphocytes, showed the highest correlation with *UBA7* expression among all examined chemokines and chemokine receptors (Supplementary Fig. S4C). Therefore, we hypothesized that the tumor-suppressive effect of *UBA7* might be further reinforced by T lymphocytes in the TME.

To advance this hypothesis, we asked whether the observation made in patients with breast cancer could be mirrored in our MMTV–PyVmT breast cancer model. We first performed detailed analysis of T-cell populations in tumors derived from these mice and observed that $CD3^+CD4^+$ and $CD3^+CD8^+$ T cells were all significantly reduced in tumors from *Uba7* KO mice compared with tumors from WT mice (Fig. 2A; Supplementary Fig. S5). In contrast, tumors from KO mice showed an increase in the percentage of $CD11b^+Gr1^-F4/80^+$ TAMs. No significant difference was observed in the percentage of intratumoral $CD11b^+Gr1^+$ cells, which could be tumor-associated neutrophils and/or myeloid-derived suppressor cells (Fig. 2A). Considering the limited role of TAMs in regulating spontaneous PyVmT tumor growth, as established earlier (17, 18), we chose to focus our efforts on understanding protein ISGylation-regulated T-cell activity in the PyVmT tumor model. Staining for CD69 (a T-cell activation marker, which is also expressed on anergic T cells) identified similar percentages of $CD3^+CD4^+$ and $CD3^+CD8^+$ T cells expressing such marker within tumors from both WT and *Uba7* KO groups (Supplementary Fig. S6A). Further analysis revealed that there was no significant difference in the percentage of effector $CD44^{hi}CD62L^{lo}$ T cells within the $CD3^+CD4^+$ or $CD3^+CD8^+$ T-cell populations in tumors from WT and KO mice (Supplementary Fig. S6B). Additional analysis further suggested that intratumoral $CD8^+$ T cells from *Uba7* KO tumors were not compromised based either on cell proliferation or on the expression of the key cytotoxic effector molecule GZMB (Supplementary Fig. S7A and S7B). We interpreted these findings to indicate that UBA7 does not directly modulate T-cell proliferation or function, but rather does so through increasing their infiltration into the tumor bed.

Because the expression of both *UBA7* and *ISG15* has been detected in tumor cells as well as in their stroma (Supplementary Fig. S8A and S8B), we next asked whether the suppressive TME was due to induced protein ISGylation in tumors versus stromal cells. We first established mouse mammary epithelial cells (MEC) from *Uba7* KO tumors. When *Uba7* KO MECs were injected into WT and *Uba7* KO mice, these cells developed tumors of similar sizes (Fig. 2B). This excludes the functional impairment of any tumor stromal cells due to lack of *Uba7* expression in this tumor model. Conversely, restored expression of *Uba7* rescued cellular protein ISGylation in MECs (Fig. 2C), which led to smaller tumors and reduced lung metastasis when these MECs were injected into the mouse mammary fat pad of WT mice (Fig. 2D and E). Notably, increased UBA7 expression did not affect cell growth when cultured *in vitro* (Supplementary Fig. S9). Meanwhile, knockdown of ISG15 in *Uba7* KO MECs did not show further impact on tumor growth *in vivo* (Supplementary Fig. S10A and S10B), implying that intervening free ISG15 in *Uba7* KO cells was insufficient to affect tumor growth. Furthermore, restored *Uba7* expression greatly increased infiltration of $CD3^+CD8^+$ cytotoxic T lymphocytes in tumors derived from these cells (Fig. 2F), and CD8 deficiency abrogated the tumor-suppressive effect of *Uba7*-mediated ISGylation (Fig. 2G). In combination, these results strongly implicate a tumor cell–autonomous function of UBA7, suggesting that protein ISGylation may regulate T-lymphocyte activities through a paracrine effect within the TME.

ISGylation Synergizes with TLR Signaling to Increase the Expression of CXCR3 Ligands

Having established the tumor cell–autonomous effect, we prioritized our experimentation to understand the critical role of protein ISGylation in tumor cells. Considering the highest correlation between the expression of *UBA7* and *CXCR3* in patients with breast cancer and the established role of the *CXCL9/10/11–CXCR3* axis in the regulation of T lymphocyte trafficking and antitumor immunity (2, 7, 19), we postulated that UBA7-mediated protein ISGylation might directly modulate the *CXCL9/10/11–CXCR3* signaling axis within the TME. Therefore, we next examined whether protein ISGylation regulates the production of CXCR3 ligands. Given the documented upregulation of Toll-like receptor (TLR) signaling molecules (i.e., TLR3 and TLR4) in the MMTV–PyVmT breast cancer model (20) and their known functions in shaping anticancer immunity in human breast cancer (21, 22), we first focused on TLR4 signaling and found that TLR4 activation in combination with type I IFN priming greatly stimulated the expression of *Cxcl9/10/11* (Supplementary Fig. S11). The observed synergy between IFN and TLR4 signaling prompted us to determine whether ISGylation directly contributed to the induction of CXCR3 ligands in our MEC model. Indeed, we found that UBA7-mediated ISGylation greatly enhanced the expression of *Cxcl9/10/11* in response to TLR4 signaling in IFN-primed MECs (Fig. 3A). We further confirmed an ISGylation-dependent increase in CXCL9/10 protein secretion from mouse MECs after TLR4 activation in IFN-primed cells (Fig. 3B), although the CXCL11 protein was not detected under our conditions. We further showed that protein ISGylation also increased poly(I:C)–stimulated expression of *Cxcl9/10* (Fig. 3C and D), indicating that ISGylation synergized with both TLR3 and TLR4 signaling to increase the expression of CXCR3 ligands. In contrast, we detected little effect of ISGylation on TNFα, IL1β, or poly(dA:dT)–stimulated expression of CXCR3 ligands under investigated conditions (Supplementary

Published OnlineFirst January 23, 2020; DOI: 10.1158/2159-8290.CD-19-0608

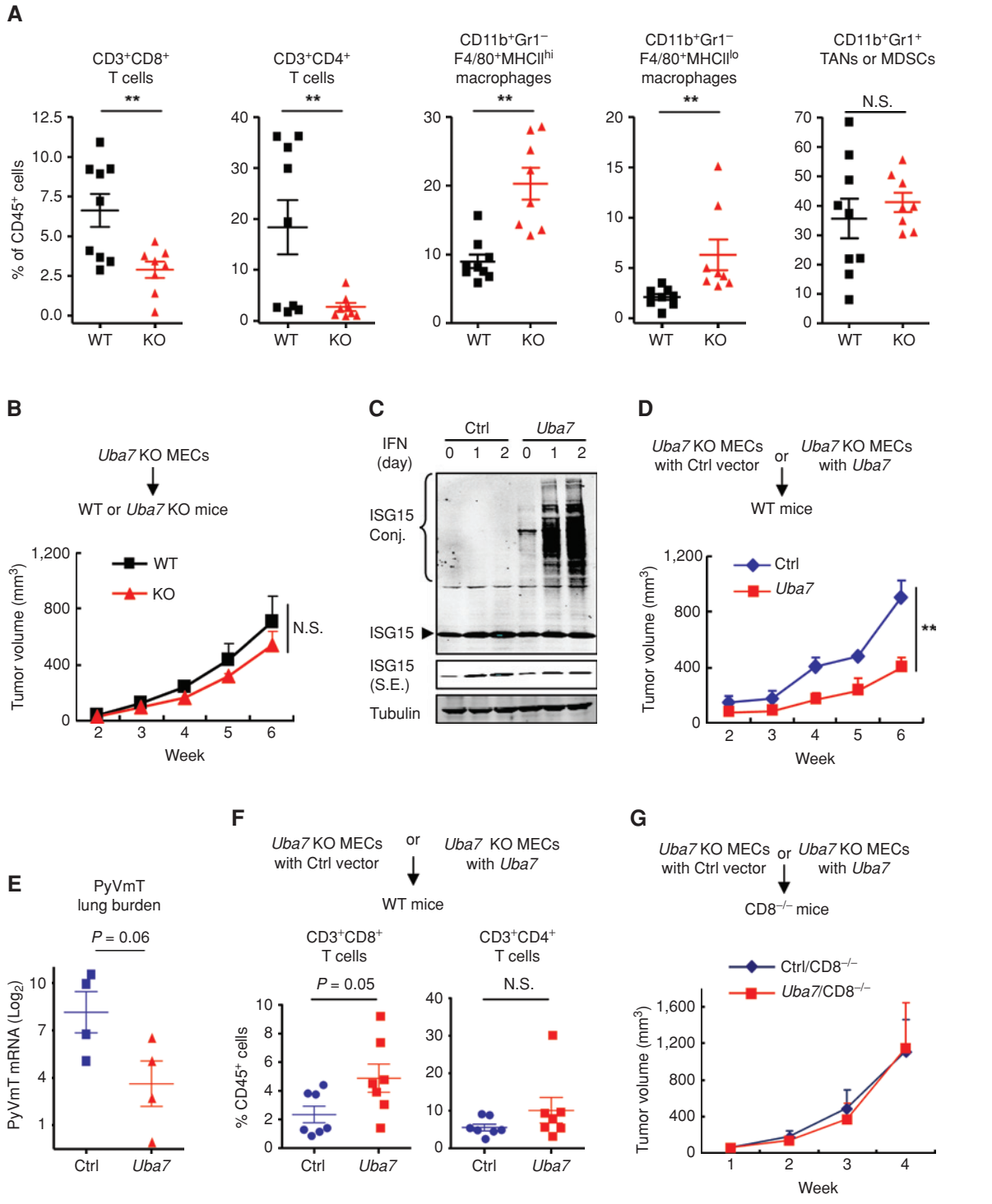

Figure 2. Protein ISGylation stimulates intratumoral infiltration of T lymphocytes. **A,** Flow cytometric analysis of intratumoral leukocytes in the tumors from PyVmT/WT and PyVmT/*Uba7* KO mice. Numbers expressed as percentages of total CD45+ leukocytes ($n = 7$–8). *P*, Student *t* test. TANs, tumor-associated neutrophils; MDSCs, myeloid-derived suppressor cells. **B,** Tumor growth from PyVmT/*Uba7* KO MECs in WT and *Uba7* KO mice (mean + SEM, $n = 5$). *P*, two-way ANOVA. **C,** Restored *Uba7* expression in PyVmT/*Uba7* KO MECs. Cells were treated by type I IFN up to 2 days, and cell lysates were immunoblotted by antibodies as indicated. S.E., short exposure. **D,** Tumor growth from PyVmT/*Uba7* KO positive control vector (henceforth "Ctrl") or PyVmT/*Uba7* KO + *Uba7* (henceforth "*Uba7*") MECs in WT mice (mean + SEM, $n = 4$). A representative set from three independent experiments ($n = 4$–5) is shown. **, $P < 0.01$, by two-way ANOVA. **E,** PyVmT lung burden in mice from **D** (mean + SEM, $n = 4$). *P*, Student *t* test. **F,** Flow cytometric analysis of CD4+ and CD8+ T cells in tumors from mice injected with Ctrl or *Uba7* MECs after week 6. Numbers expressed as percentages of total CD45+ leukocytes. Pooled data are presented from two independent experiments ($n = 7$). *P*, Student *t* test. **G,** Tumor growth from Ctrl or *Uba7* MECs in CD8-deficient mice (mean + SEM, $n = 6$).

Published OnlineFirst January 23, 2020; DOI: 10.1158/2159-8290.CD-19-0608

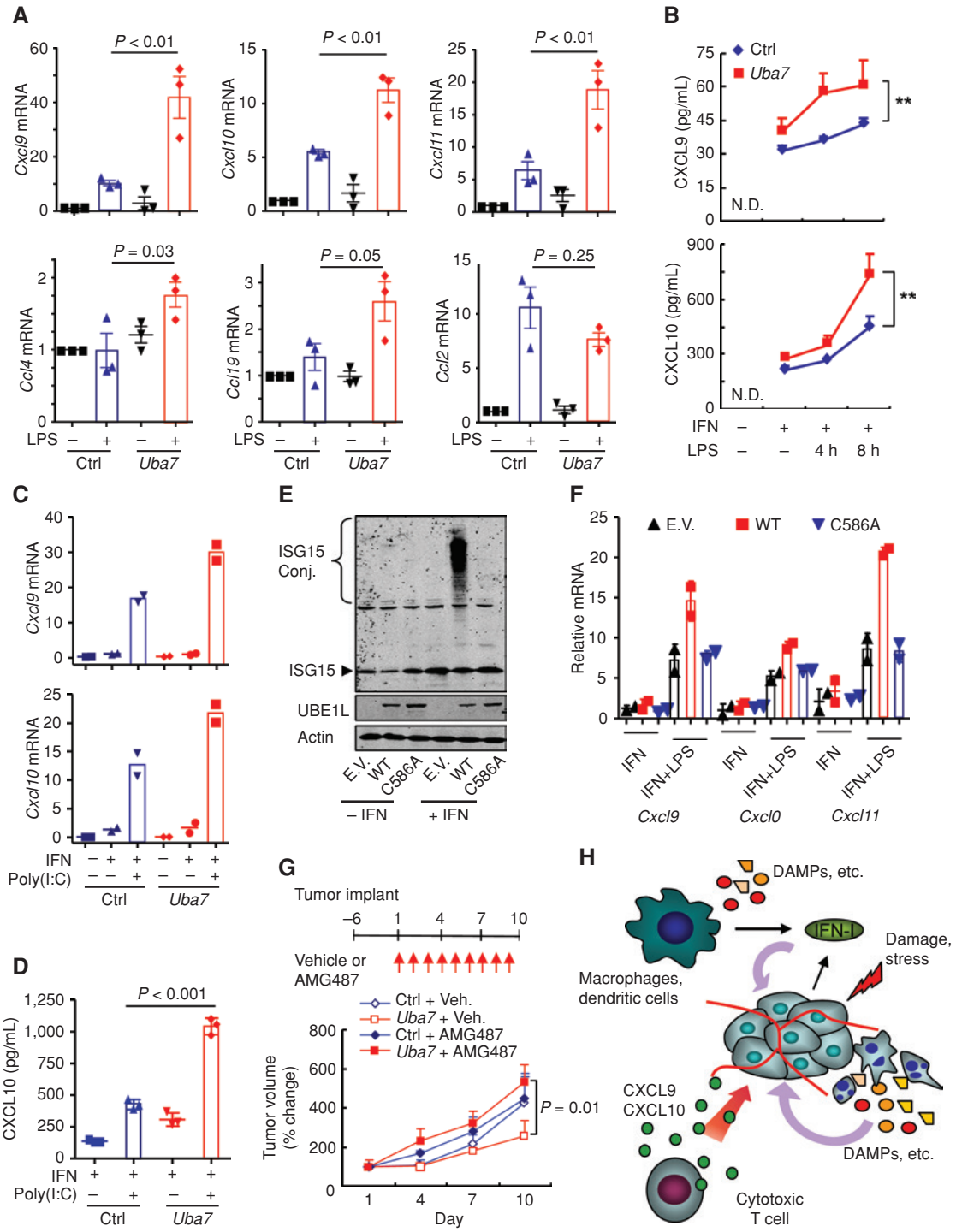

Figure 3. ISGylation synergizes with TLR signaling to increase expression of CXCR3 ligands. **A,** RT-qPCR analyzing expression of multiple chemokine genes in IFN-primed Ctrl or *Uba7* MECs after TLR4 activation (mean + SEM, $n = 3$). *P*, one-way ANOVA *post hoc* Tukey test. **B,** Secreted CXCL9/10 in the supernatant from Ctrl or *Uba7* MECs by ELISA (mean + SD, $n = 3$). **, $P < 0.01$, two-way ANOVA. N.D., not detected. **C,** RT-qPCR analyzing expression of *Cxcl9/10* in IFN-primed Ctrl or *Uba7* MECs after poly(I:C) treatment (mean from biological duplicates). **D,** Secreted CXCL10 in the supernatant from Ctrl or *Uba7* MECs by ELISA (mean + SD, $n = 3$). *P*, one-way ANOVA *post hoc* Tukey test. **E,** Restored expression of WT and UBA7 C586A in PyVmT/*Uba7* KO MECs. Cells were treated by type I IFN (1,000 U/mL) for 24 hours, and cell lysate was immunoblotted for antibodies as indicated. **F,** RT-qPCR analysis of expression of CXCR3 ligands from empty vector (E.V.)–, WT *Uba7*–, and *Uba7*^{C586A}–expressing MECs after each perturbation (mean + SD from biological duplicates). **G,** Tumor volume changes of orthotopic tumors by Ctrl or *Uba7* MECs after treated with vehicle or AMG487 (mean + SEM, $n = 4$–5). *P*, two-way ANOVA. **H,** Model of protein ISGylation–regulated expression of CXCR3 ligands and their contribution to antitumor immunity. The presence of protein ISGylation facilitates IFN–TLR-stimulated *CXCL9/10* expression in the TME and therefore promotes CXCR3 signaling axis–guided intratumoral infiltration of cytotoxic T cells.

Published OnlineFirst January 23, 2020; DOI: 10.1158/2159-8290.CD-19-0608

Fig. S12A–S12C). Consistent with the importance of UBA7-catalyzed ISGylation in TLR-stimulated expression of *Cxcl9/10*, we found that the expression of an enzyme-deficient form of UBA7 (C586A) failed to increase the expression of CXCR3 ligands (Fig. 3E and F). Furthermore, CXCR3 blockade abrogated the tumor-suppressive effect of ISGylation (Fig. 3G). Together, these results demonstrated a vital role for cancer-autonomous protein ISGylation in facilitating cytotoxic T cell–mediated killing in breast cancer through the increased expression of CXCR3 ligands, as illustrated (Fig. 3H).

ISGylation Modulates the Function of Nuclear STATs in Chemokine Expression

With the established importance of the CXCR3 signaling axis in protein ISGylation–regulated tumor suppression, we next investigated the molecular mechanisms underlying ISGylation-facilitated CXCR3 ligand expression in response to TLR signaling in IFN-primed cells. Both TLR3 and TLR4 signaling are known to activate NFκB, MAPK, and TBK1/IKKε signaling to induce expression of many genes (23). In our experimental system, ISGylation induced by IFN priming did not seem to influence TLR4 activation–induced p38, JNK, or IRF3 phosphorylation (Supplementary Fig. S13A). Although we did observe ISGylation impaired ERK phosphorylation and increased the abundance of IKBα (an inhibitor of NFκB activation; Supplementary Fig. S13A), treatment with an ERK inhibitor, U0126, did not increase *Cxcl9/10/11* expression (Supplementary Fig. S13B). These data imply that protein ISGylation may not activate TLR4 signaling through any of the cytoplasmic TLR4 proximal signaling cascades.

Although it remains unclear exactly how TLR activation licenses gene activation in IFN-primed cells, we decided to first focus on understanding how ISGylation contributes to the IFN-primed state, which is known to be critical for induction of CXCR3 ligands. In this regard, we noted that transcription factors STAT1 and STAT2 have been implicated in the regulation of CXCL9/10/11 expression. Although nuclear translocation is the primary mechanism for STAT activation in response to IFN signaling, we found that protein ISGylation had little influence on nuclear translocation of both STAT1 and STAT2 (Supplementary Fig. S14A). This directed us to investigate the possibility that ISGylation might regulate the function of STAT1 and STAT2 within the nucleus. Interestingly, both of these STATs are themselves ISGs and subject to protein ISGylation in response to IFN treatment (Supplementary Fig. S14B). Measuring the nuclear distribution of STAT1 by stochastic optical reconstruction microscopy, we observed the ISGylation-dependent redistribution of STAT1 to form clusters of various size and density in the nucleus (Supplementary Fig. S15A–S15D). We further observed increased interaction between nuclear STAT1 and STAT2 in the presence of ISGylation (Supplementary Fig. S15E). Importantly, ISGylation significantly increased STAT2 binding to IFN-stimulated response elements (ISRE) in *Cxcl9/10* enhancers, and a similar trend was observed for STAT1 (Fig. 4A; Supplementary Fig. S15F). To determine the global impact of ISGylation on gene expression, we determined ISGylation-regulated gene expression by RNA-seq and found that the expression of a subset of IFN–TLR4 signaling–regulated genes was indeed enhanced by protein ISGylation (Supplementary Fig. S16A and S16B; Supplementary Table S2), some of which was further confirmed by RT-qPCR (Supplementary Fig. S16C). Using specific pharmaceutical inhibitors, we further found that the expression of CXCR3 ligands required coactivation of multiple signaling pathways, including the TBK1/IKKε and JAK–STAT pathways (Supplementary Fig. S17A and S17B). These data therefore attributed a subset of TLRs signaling–induced gene-expression events, including *Cxcl9* and *Cxcl10*, to ISGylation-induced clustering of STAT1 and STAT2 in the nucleus of IFN-primed cells.

ISGylation Induces a Subset of STAT Clusters to Associate with PML Bodies

Given the substantial role of protein ISGylation in gene transcription, we further examined more detailed mechanisms. The observed clustering of both STAT1 and STAT2 prompted us to consider a role for ISGylation in mediating phase separation of the transcriptional machinery, a concept recently suggested to play critical roles in controlling compartmentalization and gene expression in the nucleus (24). Notably, promyelocytic leukemia (PML) is an ISG, and PML nuclear bodies are membrane-less organelles, which can be induced by IFN signaling (25). We therefore hypothesized that protein ISGylation–mediated complex formation of STAT1 and STAT2 might also show increased association with IFN-induced PML bodies. Indeed, type I IFN dramatically induced the formation of PML bodies in MECs, although protein ISGylation did not affect the number of PML bodies (Supplementary Fig. S18A–S18C). Importantly, we found that protein ISGylation facilitated condensation of STAT1 and STAT2, especially STAT2, around IFN-induced PML bodies by expansion microscopy (Fig. 4B–D). These observations suggest that ISGylation facilitates nuclear reprogramming.

To test the functional relevance of such IFN-induced nuclear compartmentalization, we took advantage of arsenic-mediated PML degradation, as reported earlier (26), and observed that short-term treatment with arsenic trioxide depleted cellular PML protein without affecting the levels of STAT1, STAT2, or ISGylation (Supplementary Fig. S19). Importantly, however, such treatment diminished ISGylation-dependent expression of *Cxcl9/10/11* (Fig. 4E). However, *Ccl2*, whose expression is also regulated by IFN–TLR4 signaling, was not affected by either protein ISGylation or arsenic treatment (Fig. 4E), indicating that the specificity of ISGylation and PML controlled chemokine expression in our current biological context. These data thus provide evidence for STAT-dependent expression of CXCR3 ligands as a functional consequence of ISGylation-induced STAT clustering and redistribution in the nucleus. Importantly, these findings are corroborated by multiple clinical results, showing a significant association between the expression of both *UBA7* and *PML* with *CXCL9/10/11* expression and favorable overall survival (Supplementary Fig. S20A and S20B) in patients with breast cancer. Together, these results highlighted the importance of the cooperation between ISGylation and PML in facilitating expression of CXCR3 ligands, whose expressions are required for ISGylation-regulated tumor suppression.

Published OnlineFirst January 23, 2020; DOI: 10.1158/2159-8290.CD-19-0608

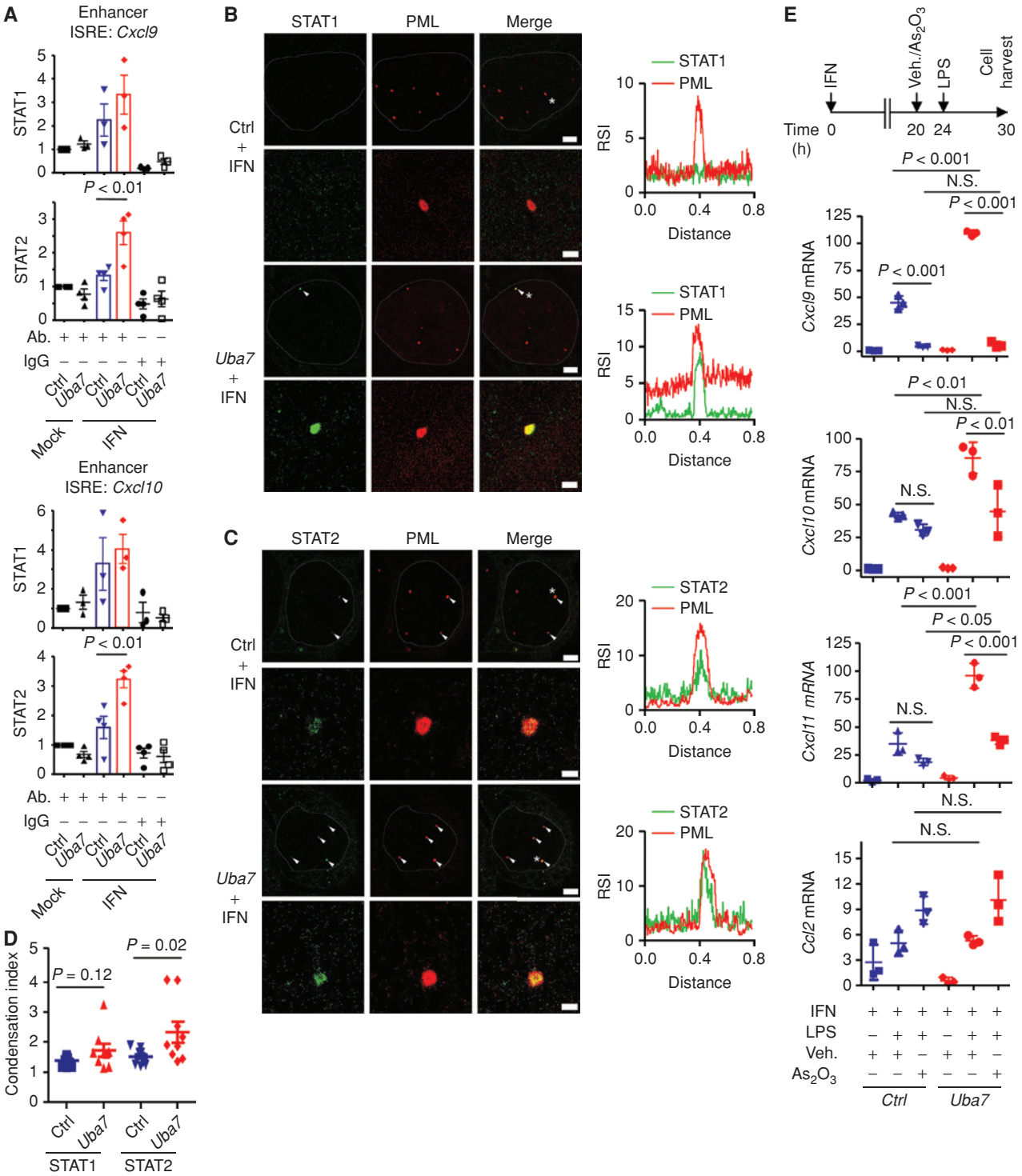

Figure 4. ISGylation and promyelocytic leukemia (PML) cooperatively modulate the function of nuclear STATs and chemokine expression. **A,** Quantitative ChIP-qPCR analysis of STAT1/STAT2 binding at enhancer ISREs of *Cxcl9/10* in Ctrl or *Uba7* MECs treated with or without IFN for 24 hours (mean + SEM, $n = 3$–4). *P*, one-way ANOVA *post hoc* Tukey test. **B** and **C,** Colocalization analysis of PML bodies (red) and STAT1 (**B**; green) and STAT2 (**C**; green) by expansion microscopy. PML bodies containing STAT1 or STAT2 were indicated by white arrows (scale bars, 2 μm). Representative PML bodies (with asterisk) with higher magnification images and their plot profiling for the relative signal intensity of each protein are shown (scale bars, 500 nm). Nucleus is outlined by dotted lines. RSI, relative signal intensity. **D,** Comparison of STAT1/STAT2 signals around the PML bodies. The condensation index was defined as ratio of the mean intensity around PML bodies to the rest of nuclei (mean ± SD, $n = 9$–11). *P*, Student *t* test. **E,** RT-qPCR analysis of chemokine-gene expression upon arsenic treatment. Ctrl or *Uba7* MECs were treated with IFN for 24 hours, and As_2O_3 or vehicle was added 4 hours prior to the LPS stimulation (mean ± SD, $n = 3$). *P*, one-way ANOVA *post hoc* Tukey test.

Published OnlineFirst January 23, 2020; DOI: 10.1158/2159-8290.CD-19-0608

DISCUSSION

Type I IFNs activate expression of hundreds of ISGs and regulate tumorigenesis and response to cancer therapy through both tumor cell–intrinsic and tumor cell–extrinsic mechanisms (5, 6). However, the roles of many individual ISGs in cancer have remained unclear. Therefore, understanding the functional interplay between ISGs may provide novel therapeutic interventions in treating human cancers. Here, we identified the ISGylation-activating enzyme *UBA7* as a key ISG in regulating malignant progression. Interestingly, nearly all of the enzymes involved in protein ISGylation, including E1, E2, E3, and the deconjugating enzyme, are ISGs themselves, suggesting their tight link to IFN-regulated cellular functions. Protein ISGylation thus affords a unique angle to look into IFN-induced gene networks that may synergistically function in the development of antitumor activities. Our current work uncovers that the IFN-inducible protein ISGylation network has an immunostimulatory function that works by facilitating CXCR3 ligand expression and cytotoxic T-cell infiltration in orchestrating a tumor-suppressive microenvironment. It is worth noting that ISGylation-induced TME also had decreased TAMs. Although TAMs are known to have a limited role in regulating spontaneous and allograft PyVmT tumor growth (17, 18, 27), they do play important roles in regulating metastatic potential (18) and response to cancer therapies in PyVmT tumors (17, 27). Thus, future studies may be geared toward understanding the contribution of protein ISGylation to regulated TAMs during tumor metastasis and/or response to cancer therapies.

Several *in vitro* studies on human cancer cell lines have revealed both positive and negative roles of protein ISGylation in breast cancer (28, 29). For example, ISG15 and protein ISGylation have been implicated in promoting invasive properties of malignant breast cancer cell lines through modulation of cytoskeletal architecture (29). On the other hand, ISGylation of ΔNp63α appears to ablate the ability of ΔNp63α to promote anchorage-independent cell growth and tumor formation (28). Although these findings collectively suggest context-dependent effects of protein ISGylation in cancer, it is important to keep in mind that IFN responses are part of the adaptive and innate immune systems in the host, thus emphasizing the importance of studying the impact of protein ISGylation on cancer progression in immunocompetent hosts. Using immunocompetent hosts, our current work highlights the importance of protein ISGylation in orchestrating a tumor-suppressive microenvironment. This mechanism is well in line with our analysis of human cancer transcriptomes and associated clinical outcomes. Although it is possible that ISGylation may enhance or suppress tumorigenesis in different contexts, just like IFN treatment, our data provide direct evidence to support the function of UBA7 as a key tumor suppressor in breast cancer. This is further corroborated by frequent deletions of chromosome 3p21.3 where *UBA7* resides in human cancer (30). Our findings suggest a mechanism underlying these genetic alterations in cancer.

We observed that the presence of protein ISGylation facilitates TLR3/4 signaling–activated CXCR3 ligand expression in our current model. TLR4 signaling is activated by a variety of ligands, including DAMPs (22, 31), and interestingly certain ISGs (e.g., IFI35, NMI) are known to function as DAMPs (32). In addition, women with breast cancer have higher relative abundance of *Bacillus, Enterobacteriaceae*, and *Staphylococcus* in their breast tissues (33), and TLR3 signaling–stimulated expressions of CXCR3 ligands have also been well characterized to play critical roles in regulating TME and antitumor immunity (19, 34). These prior observations are fully in line with the impact of loss-of-function *TLR3* or *TLR4* alleles in patients with breast cancer who relapse more quickly and show reduced overall survival after therapeutic intervention (21, 22), together indicating the importance of both TLRs in modulating anticancer immunity. Although we did not observe ISGylation-facilitated chemokine expression in the presence of poly(dA:dT) under investigated conditions, we cannot rule out the possibility that ISGylation may still contribute to signaling activation by other various endogenous stimuli, including some form of DNA released from damaged tissues, in the TME.

Our mechanistic studies have linked IFN priming to the dynamic regulation of PML bodies. PML is encoded by an ISG, and IFN signaling is known to induce the formation of PML bodies in the nucleus (25). PML has been implicated in the regulation of type I IFN–induced ISGs in cell lines, albeit with unknown mechanisms (35). Using superresolution microscopy, our current studies reveal that protein ISGylation enhances condensation of the critical transcription factors STAT1 and STAT2 and their association with PML bodies. We further observe that ISGylation-dependent chemokine expression requires the presence of PML nuclear bodies, together supporting a model in which PML nuclear bodies may contribute to the formation of a favorable nuclear environment for the expression of specific genes (36). It is entirely possible that microscopically detected PML bodies are indicative of IFN-induced condensation of both visible and invisible PML-containing complexes in the nucleus, which may underlie the IFN-induced and ISGylation-mediated gene-expression program. Our findings join the recent discovery that SUMOylation and the SUMO Interaction Motif in PML bodies contribute to multivalent interactions within PML bodies (25, 37), together suggesting that multiple post-transcriptional modifications are involved in modulating phase separation to account for the dynamic compositional control of PML bodies. It is important to point out that PML has been shown to function as a tumor suppressor in several cancer types, including breast cancer (38), but elevated PML expression has also been connected to the acquisition of aggressiveness and metastatic features in breast tumors (39). In addition, the importance of PML in regulating the immune response has been reported in a mouse model of prostate cancer (40). These seemingly contradictory observations might reflect the winning versus losing battles of the host immune system to different tumors.

The most important concept conveyed in this work is a cooperative gene network of ISGs, which is shaped by UBA7-mediated ISGylation to form a favorable nuclear environment for STAT1/2-mediated chemokine expression. These cancer cell–autonomous effects provide mechanistic insights into the regulation of cytotoxic T-cell infiltration into such TME when PRR-triggered type I IFN signaling is in synergy with activation of other inflammatory pathways, such as DAMP-induced TLR activation. Previous chromatin immunoprecipitation (ChIP) sequencing studies have shown binding of AP1, NFκB, STAT1/2, and IRF3 on enhancers of CXCR3 ligands in

Published OnlineFirst January 23, 2020; DOI: 10.1158/2159-8290.CD-19-0608

TLR-activated cells (41). Therefore, protein ISGylation–regulated clustering of STATs may facilitate their assembly on ISREs to form "enhanceosomes" (42), thereby inducing gene expression according to our working model (Supplementary Fig. S21). Importantly, by dissecting the functions of some key ISGs in this network, we suggest a potential strategy to enhance the ISGylation-induced anticancer effect through deactivating its negative regulator USP18. Such enhanced ISGylation may also help divert tumor-prone activities of ISG15 by reducing free ISG15 in the TME. This and other potential modulations of the ISG network may therefore amplify the antitumor effects of IFN-based cancer therapies, while limiting other cancer-promoting events.

METHODS

Animals and Tumor Monitoring

All experimental protocols were approved by the Institutional Animal Care and Use Committee of the University of California, San Diego (UCSD). All mice were housed and bred at the vivarium of the Moores Cancer Center at UCSD. *Uba7* KO mice were back-crossed to FVB mice over ten generations. CD8 KO mice with FVB background were kindly provided by Dr. Michael Karin (UCSD). USP18$^{C61A/C61A}$ mice in C57BL/6 background were generated by Dr. Knobeloch Klaus-Peter (University of Freiburg). FVB mice expressing *PyVmT* under the control of the mouse MMTV-LTR were crossed with WT or *Uba7* KO mice. Female mice heterozygous for the *PyVmT* transgene and homozygous-null or homozygous WT for *Uba7* were studied. C57BL/6 mice expressing *PyVmT* under the control of the mouse MMTV-LTR were crossed with WT or USP18$^{C61A/C61A}$ mice. Female mice heterozygous for the *PyVmT* transgene and WT or homozygous for USP18$^{C61A/C61A}$ were studied. Female mice were palpated twice weekly to monitor the development of mammary tumors. Tumor-bearing mice were sacrificed for analysis at endpoint, which was 13 weeks (FVB) and 22 weeks (C57BL/6) of age after birth or whenever tumor burden reached 20%. Approximate tumor volumes were calculated by the formula $4/3 \times 3.14 \times (\text{long diameter}/2) \times (\text{short diameter}/2)^2$. For metastasis studies, mouse lungs were harvested at endpoint, and the number of lung metastases was determined by hematoxylin and eosin staining of ten serial lung sections per mouse. All studies were carried out following the NIH guidelines for the care and treatment of experimental laboratory rodents.

Isolation of Mammary Tumor Cells for Flow Cytometric Analysis and Establishment of Epithelial Mammary Cell Lines

Single-cell suspensions were established from spontaneous mammary tumors arising in FVB MMTV–PyVmT females as previously described (43). Tumors were minced and incubated at 37°C for 2 hours in 5 mL of Ham's F-12K medium containing 1 mg/mL collagenase (Roche), 2 mg/mL soybean trypsin inhibitor (Sigma), and 2% BSA. After addition of fetal calf serum (FCS)–containing medium, the suspension was passed through a 70-mm nylon filter (Fisher Scientific). Single cells were pelleted by centrifugation and resuspended in PBS/2% BSA for immediate flow cytometric analysis. Stained cells were analyzed by a FACS Canto cytometer (BD Biosciences). Antibodies for flow cytometric analysis are listed in the Supplementary Table S3. For establishment of MEC cell lines, cells were cultured in DMEM/F-12 (1:1) medium mix containing 5% FCS, 2.5 mg/mL amphotericin B, 10 mg/mL penicillin–streptomycin, and MITO+ (BD Biosciences). Nonepithelial cells were removed by differential passaging, and epithelial origin of established cell lines was confirmed by CD326 (Biolegend) staining after five passages (CD326$^+$ > 98%). The cell lines have been tested as *Mycoplasma*-free using Mycosensor PCR assay kit (Agilent Technologies), with the latest test in 2018. The cell-line authentication was not routinely performed. The cells were used within 2 months after thawing.

Orthotopic Injections into the Mammary Fat Pad

In vitro–cultured MECs (1×10^6) resuspended in 1 mg/mL Matrigel (Corning) solution were injected into the abdominal mammary fat pads of female mice. Growing tumors were monitored once a week with a caliper. Approximate tumor volumes were calculated by the formula $4/3 \times 3.14 \times (\text{long diameter}/2) \times (\text{short diameter}/2)^2$.

Proteins, Chemicals, and Antibodies

Universal type I IFN was purchased from PBL Biomedical Laboratories. Cells were generally treated by IFN at 1,000 U/mL or as specified. Recombinant murine TNFα and IL1β were purchased from Peprotech. LPS was purchased from List Biological Laboratories, Inc. MEK/ERK inhibitor U0126 and TBK1/IKKε inhibitor MRT67307 were purchased from Selleckchem. Polyinosinic-polycytidylic acid sodium salt [poly(I:C)], Arsenic(III) Oxide and JAK inhibitor I were purchased from Sigma-Aldrich. Poly(dA:dT)/LyoVec was purchased from Invivogen. Antibodies used in Western blot analyses, Tubulin (Sigma-Aldrich), β-actin (Sigma-Aldrich), p-p38 (Cell Signaling Technology), p-JNK (Cell Signaling Technology), and IkBα (Biolegend), were purchased from the respective manufacturers. Rabbit anti-mouse ISG15 polyclonal antibodies have been described previously (44). Fc blocker (anti-CD16/32) was purchased from eBioscience. A full list of antibodies is shown in Supplementary Table S3.

Plasmids

FLAG-mUBA7 and mUBA7 C586A cDNA was cloned into pMSCV-puro (Clontech). All the constructs were confirmed by DNA sequencing. shRNA plasmids (pLKO.1 vectors) for m*Isg15* (TRCN0000077333 and TRCN TRCN0000077334) and control were obtained from The RNAi Consortium.

Cell Culture, Transfections, and Infection

The 293T cells have been purchased from the ATCC and authenticated by this organization with certificates and been tested as *Mycoplasma*-free using Mycosensor PCR assay kit (Agilent Technologies), with the latest test in 2018. HEK293T cells were cultured in DMEM (Invitrogen) with 10% bovine calf serum (HyClone), 2 mmol/L L-glutamine (Invitrogen), and penicillin–streptomycin (100 U/mL, Invitrogen) and were used within 2 months after thawing. Cells were transfected using polyethylenimine (PEI) reagent as previously reported (45). For *Uba7* expression in *Uba7* KO MECs, 293T cells were transfected with pMSCV-mUBA7 and pIK6.1MCV ecopac using PEI reagent. Retroviruses from the culture medium of these cells were infected to *Uba7* KO MECs, and stable infected cells were selected by puromycin (1 μg/mL).

RNA Isolation and RT-qPCR Analysis

Total RNA from tumor tissue or MECs was isolated using Trizol reagent (ThermoFisher) according to the manufacturer's instructions. For RT-qPCR analyses, equal amounts of RNA were reverse-transcribed by First Strand cDNA Synthesis Kit (MCLAB), and the resulting cDNA templates were subjected to RT-qPCR using SYBR Green detection system (Kapa Biosystems) on the CFX96 thermal cycler (Bio-Rad). Primer sequences are listed in Supplementary Table S4.

ChIP-qPCR Analysis

ChIP was performed as described previously (46). A total of 1 μg anti-STAT2 (Cell Signaling Technology) and 2 μg anti-STAT1 (Santa Cruz Biotechnology) antibodies were used per ChIP reaction. ChIP data were expressed as a percentage of input and presented as the relative fold enrichment compared with mock control. Primers used for qPCR of ISRE regions of CXCL9/10 are listed in Supplementary Table S5.

Published OnlineFirst January 23, 2020; DOI: 10.1158/2159-8290.CD-19-0608

Sandwich ELISA

For CXCL9/10/11 ELISA, MECs were seeded onto a 6-well plate, and supernatants were collected at different time points as indicated, spun down to remove debris, and analyzed according to the manufacturer's protocol (R&D Systems).

Sample Preparation, Image Acquisition, and Data Analysis for Expansion Microscopy

Cells were cultured on 18 × 18 mm-1.5 microscope cover glass (Fisher Scientific) in 12-well plates. After IFN treatment, cells were fixed in 3.7% formaldehyde, permeabilized with 0.1% Triton X-100, and blocked with 2 mg/mL BSA. Samples were incubated with primary antibodies against STAT1 (2 μg/mL), STAT2 (2 μg/mL), and PML (10 μg/mL) in blocking buffer at 4°C overnight. The procedure for sample gelation, digestion, and expansion was conducted as previously reported (47–49). Briefly, the samples were incubated in 0.01% acrylic acid *N*-hydroxysuccinimide ester (Santa Cruz Biotechnology) in PBS for 2.5 hours. A monomer solution [1x PBS, 2 mol/L NaCl, 25% sodium acrylate (w/w), 4% acrylamide (w/w), 0.04% (w/w) *N,N′*-methylenebisacrylamide] was mixed with 0.2% (w/w) ammonium persulfate (APS) and 0.2% (w/w) tetramethylethylenediamine (TEMED) to promote polymerization. The monomer solution mixed with the APS and TEMED was then added to samples to a depth of 2 mm and incubated for 2 hours at 37°C to allow for the completed polymerization. The size of the gel was measured. The polymerized gel was then immersed in 4 mL of 0.2 mg/mL proteinase K (Roche) in digestion buffer (50 mmol/L Tris, pH 8, 2 mmol/L $CaCl_2$, 3 mol/L NaCl, 0.5% Triton X-100, and 0.8 mol/L guanidine HCl) and incubated at 37°C for 3 hours. Digested gels were next placed in excess volumes of PBS for 2 hours. The gels were then stained with Alexa488- or Alexa568-conjugated secondary antibodies at room temperature overnight, followed by washing in10 mmol/L Tris buffer (pH 8.0), which achieved expansion ratio around 4 in each dimension. The expanded hydrogels were then placed onto poly-L-lysine–coated cover glass for confocal imaging.

The confocal data were analyzed by ImageJ/Fiji. For each z-stack image, the nucleus region was first identified by Gaussian blurring the DAPI channel with 1 μm interval followed by thresholding and binarization. Then, PML bodies in each nucleus were identified by Gaussian blurring the PML channel signals with interval of 140 nm, followed by thresholding and binarization. STAT1/STAT2 signals within and outside of the PML body regions were compared, with the condensation index defined as ratio of the mean intensity within PML bodies to that outside of PML bodies in nuclei. A total of 9 to 11 cells in each sample conditions were analyzed.

Quantification and Statistical Analysis

Experiments were repeated at least twice. Results are expressed as mean + SD or SEM as indicated. Statistical significance was evaluated by a paired or unpaired *t* test, or by one-way/two-way ANOVA as indicated in the figure legends, using $P < 0.05$ as indicative of statistical significance. Linear regression analyses in breast-invasive carcinoma were performed by RStudio using TCGA datasets. Data for *ISG15*-, *MX1*-, and *UBA7*-correlated genes were downloaded from cBioPotal (50, 51). The gene-expression data and survival information of 3554 patients were downloaded from the Gene Expression Omnibus (GEO) and analyzed as previously reported (52). Survival analysis was performed by drawing a Kaplan–Meier survival plot and computing a Cox proportional hazard regression as described previously (53). RNA-seq data analyzed in this study are available from GEO (GSE112532).

Disclosure of Potential Conflicts of Interest

No potential conflicts of interest were disclosed.

Authors' Contributions

Conception and design: J.-B. Fan, C. Burkart, D.-E. Zhang
Development of methodology: J.-B. Fan, S. Miyauchi, D.-E. Zhang
Acquisition of data (provided animals, acquired and managed patients, provided facilities, etc.): J.-B. Fan, S. Miyauchi, H.-Z. Xu, D. Liu, H. Cheng, M. Yan, K.-P. Knobeloch, J.N. Rich, D.-E. Zhang
Analysis and interpretation of data (e.g., statistical analysis, biostatistics, computational analysis): J.-B. Fan, S. Miyauchi, H.-Z. Xu, L.J.Y. Kim, K.-i. Arimoto, M. Yan, Y. Zhou, B. Győrffy, D.-E. Zhang
Writing, review, and/or revision of the manuscript: J.-B. Fan, B. Győrffy, J.N. Rich, X.-D. Fu, D.-E. Zhang
Administrative, technical, or material support (i.e., reporting or organizing data, constructing databases): D.-E. Zhang
Study supervision: J.-B. Fan, H. Cang, D.-E. Zhang

Acknowledgments

We thank Dr. Sam Stoner for critical editing of this manuscript, and Dr. Judith Varner and all the members of the D.-E. Zhang laboratory for discussion, suggestions, and help. We gratefully acknowledge Drs. Ernest Borden and Deborah Lenschow for ISG15 antibodies, Dr. Lesley G. Ellies for C57BL/6 and FVB/N-Tg (MMTV–PyVmT) 634Mul/J mice, and Dr. Michael Karin for CD8 KO mice. This work was supported by funding from the NIH New Innovator Award to H. Cang (1-DP2-EB020400) and funding from NIH to D.-E. Zhang (R01CA177305).

The costs of publication of this article were defrayed in part by the payment of page charges. This article must therefore be hereby marked *advertisement* in accordance with 18 U.S.C. Section 1734 solely to indicate this fact.

Received May 28, 2019; revised November 15, 2019; accepted January 17, 2020; published first January 23, 2020.

REFERENCES

1. Patel SA, Minn AJ. Combination cancer therapy with immune checkpoint blockade: mechanisms and strategies. Immunity 2018;48:417–33.
2. Spranger S, Gajewski TF. Impact of oncogenic pathways on evasion of antitumour immune responses. Nat Rev Cancer 2018;18:139–47.
3. Stark GR, Darnell JE. The JAK-STAT pathway at twenty. Immunity 2012;36:503–14.
4. Borden EC. Interferons alpha and beta in cancer: therapeutic opportunities from new insights. Nat Rev Drug Discov 2019;18:219–34.
5. Parker BS, Rautela J, Hertzog PJ. Antitumour actions of interferons: implications for cancer therapy. Nat Rev Cancer 2016;16:131–44.
6. Zitvogel L, Galluzzi L, Kepp O, Smyth MJ, Kroemer G. Type I interferons in anticancer immunity. Nat Rev Immunol 2015;15:405–14.
7. Corrales L, Matson V, Flood B, Spranger S, Gajewski TF. Innate immune signaling and regulation in cancer immunotherapy. Cell Res 2017;27:96–108.
8. Benci JL, Xu BH, Qiu Y, Wu TJ, Dada H, Twyman-Saint Victor C, et al. Tumor interferon signaling regulates a multigenic resistance program to immune checkpoint blockade. Cell 2016;167:1540–54.
9. Minn AJ, Wherry EJ. Combination cancer therapies with immune checkpoint blockade: convergence on interferon signaling. Cell 2016;165:272–5.
10. Yuan WM, Krug RM. Influenza B virus NS1 protein inhibits conjugation of the interferon (IFN)-induced ubiquitin-like ISG15 protein. EMBO J 2001;20:362–71.
11. Bektas N, Noetzel E, Veeck J, Press MF, Kristiansen G, Naami A, et al. The ubiquitin-like molecule interferon-stimulated gene 15 (ISG15) is a potential prognostic marker in human breast cancer. Breast Cancer Res 2008;10:R58.

Published OnlineFirst January 23, 2020; DOI: 10.1158/2159-8290.CD-19-0608

12. Zhang XQ, Bogunovic D, Payelle-Brogard B, Francois-Newton V, Speer SD, Yuan C, et al. Human intracellular ISG15 prevents interferon-alpha/beta over-amplification and auto-inflammation. Nature 2015;517:89–93.
13. De Palma M, Mazzieri R, Politi LS, Pucci F, Zonari E, Sitia G, et al. Tumor-targeted interferon-alpha delivery by Tie2-expressing monocytes inhibits tumor growth and metastasis. Cancer Cell 2008;14:299–311.
14. Escobar G, Moi D, Ranghetti A, Ozkal-Baydin P, Squadrito ML, Kajaste-Rudnitski A, et al. Genetic engineering of hematopoiesis for targeted IFN-alpha delivery inhibits breast cancer progression. Sci Transl Med 2014;6:217ra3.
15. Cai Y, Nogales-Cadenas R, Zhang QW, Lin JR, Zhang W, O'Brien K, et al. Transcriptomic dynamics of breast cancer progression in the MMTV-PyMT mouse model. BMC Genomics 2017;18:185.
16. Ketscher L, Hannss R, Morales DJ, Basters A, Guerra S, Goldmann T, et al. Selective inactivation of USP18 isopeptidase activity in vivo enhances ISG15 conjugation and viral resistance. Proc Natl Acad Sci U S A 2015;112:1577–82.
17. Ruffell B, Chang-Strachan D, Chan V, Rosenbusch A, Ho CMT, Pryer N, et al. Macrophage IL-10 blocks CD8(+) T cell-dependent responses to chemotherapy by suppressing IL-12 expression in intratumoral dendritic cells. Cancer Cell 2014;26:623–37.
18. Lin EY, Nguyen AV, Russell RG, Pollard JW. Colony-stimulating factor 1 promotes progression of mammary tumors to malignancy. J Exp Med 2001;193:727–39.
19. Sistigu A, Yamazaki T, Vacchelli E, Chaba K, Enot DP, Adam J, et al. Cancer cell-autonomous contribution of type I interferon signaling to the efficacy of chemotherapy. Nat Med 2014;20:1301–9.
20. Lee SH, Jia SD, Zhu YN, Utermark T, Signoretti S, Loda M, et al. Transgenic expression of polyomavirus middle T antigen in the mouse prostate gives rise to carcinoma. J Virol 2011;85:5581–92.
21. Vacchelli E, Enot DP, Pietrocola F, Zitvogel L, Kroemer G. Impact of pattern recognition receptors on the prognosis of breast cancer patients undergoing adjuvant chemotherapy. Cancer Res 2016;76:3122–6.
22. Apetoh L, Ghiringhelli F, Tesniere A, Obeid M, Ortiz C, Criollo A, et al. Toll-like receptor 4-dependent contribution of the immune system to anticancer chemotherapy and radiotherapy. Nat Med 2007;13:1050–9.
23. Kawasaki T, Kawai T. Toll-like receptor signaling pathways. Front Immunol 2014;5:461.
24. Hnisz D, Shrinivas K, Young RA, Chakraborty AK, Sharp PA. A phase separation model for transcriptional control. Cell 2017;169:13–23.
25. Lallemand-Breitenbach V, de The H. PML nuclear bodies: from architecture to function. Curr Opin Cell Biol 2018;52:154–61.
26. Zhang XW, Yan XJ, Zhou ZR, Yang FF, Wu ZY, Sun HB, et al. Arsenic trioxide controls the fate of the PML-RAR alpha oncoprotein by directly binding PML. Science 2010;328:240–3.
27. Shiao SL, Ruffell B, DeNardo DG, Faddegon BA, Park CC, Coussens LM. TH(H)2-polarized CD4(+) T cells and macrophages limit efficacy of radiotherapy. Cancer Immunol Res 2015;3:518–25.
28. Jeon YJ, Jo MG, Yoo HM, Hong SH, Park JM, Ka SH, et al. Chemosensitivity is controlled by p63 modification with ubiquitin-like protein ISG15. J Clin Invest 2012;122:2622–36.
29. Desai SD, Reed RE, Burks J, Wood LM, Pullikuth AK, Haas AL, et al. ISG15 disrupts cytoskeletal architecture and promotes motility in human breast cancer cells. Exp Biol Med 2012;237:38–49.
30. Sekido Y, Ahmadian M, Wistuba II, Latif F, Bader S, Wei MH, et al. Cloning of a breast cancer homozygous deletion junction narrows the region of search for a 3p21.3 tumor suppressor gene. Oncogene 1998;16:3151–7.
31. Haricharan S, Brown P. TLR4 has a TP53-dependent dual role in regulating breast cancer cell growth. Proc Natl Acad Sci U S A 2015;112:E3216–E25.
32. Xiahou ZK, Wang XL, Shen J, Zhu XX, Xu F, Hu R, et al. NMI and IFP35 serve as proinflammatory DAMPs during cellular infection and injury. Nat Commun 2017;8:950.
33. Urbaniak C, Gloor GB, Brackstone M, Scott L, Tangney M, Reid G. The microbiota of breast tissue and its association with breast cancer. Appl Environ Microbiol 2016;82:5039–48.
34. Salaun B, Zitvogel L, Asselin-Paturel C, Morel Y, Chemin K, Dubois C, et al. TLR3 as a biomarker for the therapeutic efficacy of double-stranded RNA in breast cancer. Cancer Res 2011;71:1607–14.
35. Kim YE, Ahn JH. Positive role of promyelocytic leukemia protein in type I interferon response and its regulation by human cytomegalovirus. PLoS Pathog 2015;11:e1004785.
36. Boisvert FM, Hendzel MJ, Bazett-Jones DP. Promyelocytic leukemia (PML) nuclear bodies are protein structures that do not accumulate RNA. J Cell Biol 2000;148:283–92.
37. Banani SF, Rice AM, Peeples WB, Lin Y, Jain S, Parker R, et al. Compositional control of phase-separated cellular bodies. Cell 2016;166:651–63.
38. Salomoni P, Pandolfi PP. The role of PML in tumor suppression. Cell 2002;108:165–70.
39. Martin-Martin N, Piva M, Urosevic J, Aldaz P, Sutherland JD, Fernandez-Ruiz S, et al. Stratification and therapeutic potential of PML in metastatic breast cancer. Nat Commun 2016;7:12595.
40. Bezzi M, Seitzer N, Ishikawa T, Reschke M, Chen M, Wang GC, et al. Diverse genetic-driven immune landscapes dictate tumor progression through distinct mechanisms. Nat Med 2018;24:165–75.
41. Kaikkonen MU, Spann NJ, Heinz S, Romanoski CE, Allison KA, Stender JD, et al. Remodeling of the enhancer landscape during macrophage activation is coupled to enhancer transcription. Mol Cell 2013;51:310–25.
42. Au-Yeung N, Horvath CM. Transcriptional and chromatin regulation in interferon and innate antiviral gene expression. Cytokine Growth Factor Rev 2018;44:11–7.
43. Burkart C, Arimoto KI, Tang TD, Cong XL, Xiao NM, Liu YC, et al. Usp18 deficient mammary epithelial cells create an antitumour environment driven by hypersensitivity to IFN-lambda and elevated secretion of Cxcl10. EMBO Mol Med 2013;5:1035–50.
44. Malakhova OA, Yan M, Malakhov MP, Yuan YZ, Ritchie KJ, Kim KI, et al. Protein ISGylation modulates the JAK-STAT signaling pathway. Genes Dev 2003;17:455–60.
45. Longo PA, Kavran JM, Kim MS, Leahy DJ. Transient mammalian cell transfection with polyethylenimine (PEI). Methods Enzymol 2013;529:227–40.
46. Deliard S, Zhao JH, Xia QH, Grant SFA. Generation of high quality chromatin immunoprecipitation DNA template for high-throughput sequencing (ChIP-seq). J Vis Exp 2013;74:e50286.
47. Chozinski TJ, Halpern AR, Okawa H, Kim HJ, Tremel GJ, Wong ROL, et al. Expansion microscopy with conventional antibodies and fluorescent proteins. Nat Methods 2016;13:485–8.
48. Tillberg PW, Chen F, Piatkevich KD, Zhao YX, Yu CC, English BP, et al. Protein-retention expansion microscopy of cells and tissues labeled using standard fluorescent proteins and antibodies. Nat Biotechnol 2016;34:987–92.
49. Chen F, Tillberg PW, Boyden ES. Expansion microscopy. Science 2015;347:543–8.
50. Gao JJ, Aksoy BA, Dogrusoz U, Dresdner G, Gross B, Sumer SO, et al. Integrative analysis of complex cancer genomics and clinical profiles using the cBioPortal. Sci Signal 2013;6:pl1.
51. Cerami E, Gao JJ, Dogrusoz U, Gross BE, Sumer SO, Aksoy BA, et al. The cBio cancer genomics portal: an open platform for exploring multidimensional cancer genomics data. Cancer Discov 2012;2:401–4.
52. Gyorffy B, Lanczky A, Eklund AC, Denkert C, Budczies J, Li QY, et al. An online survival analysis tool to rapidly assess the effect of 22,277 genes on breast cancer prognosis using microarray data of 1,809 patients. Breast Cancer Res Treat 2010;123:725–31.
53. Gyorffy B, Lanczky A, Szallasi Z. Implementing an online tool for genome-wide validation of survival-associated biomarkers in ovarian-cancer using microarray data from 1287 patients. Endocr Relat Cancer 2012;19:197–208.

Published OnlineFirst January 23, 2020; DOI: 10.1158/2159-8290.CD-19-0608

AACR American Association for Cancer Research

CANCER DISCOVERY

Type I Interferon Regulates a Coordinated Gene Network to Enhance Cytotoxic T Cell–Mediated Tumor Killing

Jun-Bao Fan, Sayuri Miyauchi, Hui-Zhong Xu, et al.

Cancer Discov 2020;10:382-393. Published OnlineFirst January 23, 2020.